

This article was downloaded by: [Efthymios Papadopoulos]

On: 09 February 2015, At: 13:19

Publisher: Taylor & Francis

Informa Ltd Registered in England and Wales Registered Number: 1072954 Registered office: Mortimer House, 37-41 Mortimer Street, London W1T 3JH, UK



International Journal of Pavement Engineering

Publication details, including instructions for authors and subscription information:

<http://www.tandfonline.com/loi/gpav20>

Analysis of inverted base pavements with thin-asphalt layers

E. Papadopoulos^a & J.C. Santamarina^a

^a Department of Civil and Environmental Engineering, Georgia Institute of Technology, 790 Atlantic Drive, Suite 2131A, Atlanta, GA 30332, USA

Published online: 06 Feb 2015.



[Click for updates](#)

To cite this article: E. Papadopoulos & J.C. Santamarina (2015): Analysis of inverted base pavements with thin-asphalt layers, International Journal of Pavement Engineering, DOI: [10.1080/10298436.2015.1007232](https://doi.org/10.1080/10298436.2015.1007232)

To link to this article: <http://dx.doi.org/10.1080/10298436.2015.1007232>

PLEASE SCROLL DOWN FOR ARTICLE

Taylor & Francis makes every effort to ensure the accuracy of all the information (the "Content") contained in the publications on our platform. However, Taylor & Francis, our agents, and our licensors make no representations or warranties whatsoever as to the accuracy, completeness, or suitability for any purpose of the Content. Any opinions and views expressed in this publication are the opinions and views of the authors, and are not the views of or endorsed by Taylor & Francis. The accuracy of the Content should not be relied upon and should be independently verified with primary sources of information. Taylor and Francis shall not be liable for any losses, actions, claims, proceedings, demands, costs, expenses, damages, and other liabilities whatsoever or howsoever caused arising directly or indirectly in connection with, in relation to or arising out of the use of the Content.

This article may be used for research, teaching, and private study purposes. Any substantial or systematic reproduction, redistribution, reselling, loan, sub-licensing, systematic supply, or distribution in any form to anyone is expressly forbidden. Terms & Conditions of access and use can be found at <http://www.tandfonline.com/page/terms-and-conditions>

Analysis of inverted base pavements with thin-asphalt layers[†]

E. Papadopoulos* and J.C. Santamarina

Department of Civil and Environmental Engineering, Georgia Institute of Technology, 790 Atlantic Drive, Suite 2131A, Atlanta, GA 30332, USA

(Received 3 December 2014; accepted 15 December 2014)

Inverted base pavements are flexible pavement structures built by placing a top quality compacted granular aggregate base between a rigid cement-treated base and a thin-asphalt surface layer. The proximity of the granular base to the load makes its behaviour critical to the pavement response. Three-dimensional finite-element simulations are conducted to assess the mechanical performance of different inverted base pavement structures, with emphasis placed on pavements that feature thin-asphalt surface layers. A nonlinear constitutive model captures the anisotropic stress-dependent stiffness of the granular base. Results show that the stress distribution within inverted base pavements is markedly different from that of conventional pavements due to the stiffness contrast between successive layers. Thin-asphalt layers deform more uniformly and experience lower tension than thick layers. However, in the presence of combined shear and vertical contact loads, the benefits of a membrane response in thin asphalt concrete layers may be overwhelmed by the increased tensile strain at the load edge. The transition from beam to membrane asphalt response depends on the relative stiffness between the asphalt layer and the aggregate base. In most cases, the transition takes place at an asphalt layer thickness between 25 mm and 50 mm.

Keywords: pavement modelling; constitutive model; inverted base pavement; anisotropy; finite-element model; granular base

1. Introduction

Inverted base pavements are flexible pavement structures where the granular aggregate base (GAB) is placed between a cement-treated base (CTB) and an asphalt concrete surface layer asphalt concrete (AC). Inverted base pavements have been used in other countries, particularly South Africa (Tutumluer 2013, Papadopoulos and Santamarina 2015). Yet, the experience with full-scale inverted base pavements in the USA remains limited to a few cases (Terrell *et al.* 2003, Cortes and Santamarina 2013, Papadopoulos *et al.* 2015).

Mechanistic methodologies help analyse the pavement response to traffic loads which is subsequently linked to their expected life (NCHRP 2004). Mechanistic analyses are necessary for the evaluation of unconventional pavement structures, such as inverted base pavements, that lack the extensive empirical evidence accumulated for conventional pavements.

Early mechanistic analyses were conducted using closed-form solutions of multi-layer elastic systems (Burmister *et al.* 1943, Burmister 1945). Finite-element codes were first used to analyse pavement structures in the late 1960s (Duncan *et al.* 1968). Several computer programmes have been specifically developed for pavement analysis since then (Raad and Figueroa 1980, Brown and Pappin 1981; Barksdale *et al.* 1989, Tutumluer and

Barksdale 1995, Park and Lytton 2004). In the meantime, there have been important advances in constitutive models for pavement analysis, including anisotropic models for granular bases, nonlinear stiffness for the subgrade and the granular base, elasto–viscoplastic behaviour for the asphalt layers and realistic tyre–pavement contact stress (Al-Qadi *et al.* 2010, Liu and Shalaby 2013).

In this study, the behaviour of inverted base pavements is analysed through a mechanistic pavement response model built on the finite-element code ABAQUS, augmented with user-defined subroutines (Yoo *et al.* 2006, Kim *et al.* 2009, Cortes *et al.* 2012). In particular, a nonlinear anisotropic constitutive model is used to capture the behaviour of the granular base. Different inverted base pavement designs are compared to investigate the interaction between layers and the effect of combined normal and shear contact forces.

2. Numerical approach: constitutive model

This study places special emphasis on the simulation of the GAB, given its structural contribution and proximity to traffic loads in inverted base pavements. Most numerical simulations capture the stiffness of granular layers using the resilient modulus M_r concept in a secant stiffness formulation (Tutumluer and Barksdale 1995, Yoo *et al.*

[†]Technical paper prepared for the *International Journal of Pavement Engineering*.

*Corresponding author. Email: epapadop@outlook.com

2006, Al-Qadi *et al.* 2010). Several models have been developed to predict the resilient modulus as a function of the state of stress during traffic loading (Hicks and Monismith 1971, Uzan 1985, Brown 1996).

In this study, a tangent formulation is adopted to model the resilient stress-dependent stiffness of granular bases. The tangent formulation captures the incremental material response and can model any arbitrary stress path. This model captures the stress–strain behaviour of granular bases at small and intermediate deformations using a modulus reduction rule and accounts for stress-hardening, shear-softening and both fabric and stress-induced anisotropy. Details follow.

2.1. Small-strain stiffness

Granular bases exhibit inherent anisotropy due to preferential particle alignment during compaction. Furthermore, the small-strain Young's modulus E_0^i in the direction $-i$ depends on the normal stress in the corresponding principal stress direction (Kopperman *et al.* 1982, Papadopoulos 2014), which gives rise to stress-induced anisotropy (Oda *et al.* 1985):

$$E_0^x = c_1^x \left(\frac{\sigma_{xx}}{\text{kPa}} \right)^{c_2}, \quad (1)$$

$$E_0^y = c_1^y \left(\frac{\sigma_{yy}}{\text{kPa}} \right)^{c_2}, \quad (2)$$

$$E_0^z = c_1^z \left(\frac{\sigma_{zz}}{\text{kPa}} \right)^{c_2}, \quad (3)$$

where σ_{ii} is the normal stress in the principal stress direction i , the factors c_1^i represent the stiffness at $\sigma_{ii} = 1$ kPa and the exponent c_2 captures the stress sensitivity. This model can effectively simulate both the inherent and stress-induced anisotropy of granular bases.

An orthotropic linear elastic formulation requires nine independent parameters; however, the model can be simplified by making behaviour-guided assumptions that do not diminish the ability to fit real data, yet decrease complexity (Cortes 2010). In particular, the shear stiffness in the plane ij , G_{ij} , is computed as

$$G^{ij} = \frac{0.5 \cdot (E^i + E^j)}{2.2}, \quad (4)$$

where Poisson's ratio is assumed to be $\nu = 0.1$, which is a typical value for granular materials in the small-strain regime (Santamarina *et al.* 2001).

2.2. Strain-dependent modulus degradation

The tangent stiffness E_{tan} required for the incremental finite-element formulation must reproduce shear softening as observed during deviatoric loading. The stress–strain behaviour of granular materials under deviatoric loading

generally follows a hyperbolic trend (Hardin and Drnevich 1972b, Prevost and Keane 1990, Mayne 2001). The simplest model to capture this behaviour involves two parameters: the initial stiffness E_0 and the ultimate load capacity q_u . The modified hyperbolic model used in this study includes a third parameter c_3 to capture data trends more accurately (Fahey and Carter 1993; van Niekerk *et al.* 2002):

$$\frac{E_{\text{tan}}}{E_0} = 1 - \left(\frac{q}{q_u} \right)^{c_3}, \quad (5)$$

where q is the deviatoric stress:

$$q = \frac{1}{\sqrt{2}} \cdot \sqrt{(\sigma_1 - \sigma_2)^2 + (\sigma_1 - \sigma_3)^2 + (\sigma_3 - \sigma_2)^2}. \quad (6)$$

High c_3 values correspond to more brittle materials. The shear strength q_u follows a friction law. The Drucker–Prager failure criterion is used in this study for its simplicity and numerical stability:

$$q_u = D + M \cdot p, \quad (7)$$

where D and M are functions of the cohesion intercept c and friction angle φ :

$$D = c \cdot \frac{6 \cos \varphi}{3 - \sin \varphi}, \quad (8)$$

$$M = \frac{6 \sin \varphi}{3 - \sin \varphi}, \quad (9)$$

while coarse-grained granular materials do not exhibit real cohesion, a small value of the cohesion intercept improves numerical stability under low stresses. Symmetry in the orthotropic stiffness matrix implies the following mechanical constraint between Young's moduli and Poisson's ratios in different directions:

$$\frac{E_i}{E_j} = \frac{\nu_{ij}}{\nu_{ji}}. \quad (10)$$

The values of Poisson's ratio used for calculating the stress–strain response are assumed to be $\nu_{xy} = \nu_{zy} = \nu_{zx} = 0.35$. These values are relevant for intermediate deformations away from failure ($q/q_u < 0.6$).

2.3. Numerical implementation and calibration

The constitutive model defined by Equations (1)–(10) is implemented in ABAQUS in an explicit formulation using a user-defined subroutine. The model is calibrated against true triaxial tests results (Figure 1(a), data in Papadopoulos 2014). The small-strain stiffness is determined using wave propagation measurements in both the horizontal and vertical directions. First, the small-strain parameters c_1 , c_2 are selected to satisfy experimental data. Then, the

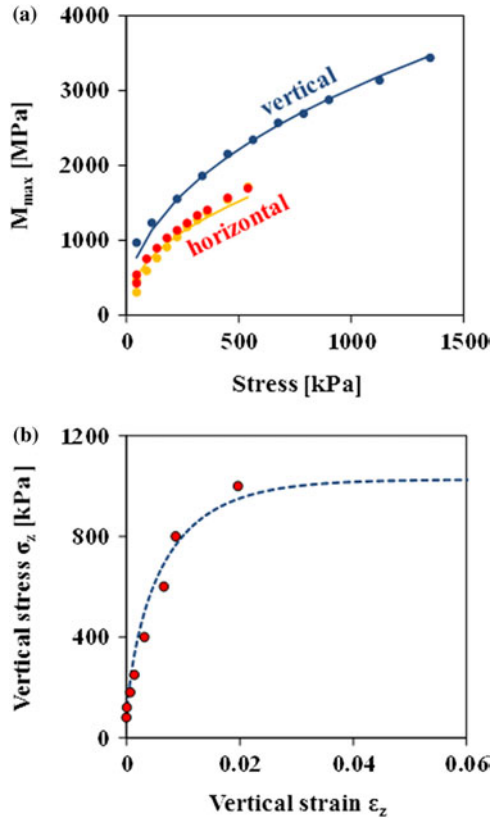


Figure 1. Calibration of the constitutive model for the GAB [Equations (1)–(10)]. (a) Small-strain constrained modulus M_{max} versus stress in the direction of P-wave propagation for horizontal and vertical wave propagation. Dots are recorded data while the line shows the fitted power equation. (b) Stress–strain response during triaxial compression; dots are data points measured in the triaxial test, and the line is the response of a one-element model simulated in ABAQUS.

modulus reduction parameters c_3 , D and M are established from triaxial test data. While the data used for calibration were obtained from quasi-static tests conducted as part of this study, strain rates similar to traffic loading are preferred for large-strain parameters, as granular materials exhibit higher strength at large strain rates (Garg and Thompson 1997, Tutumluer 2013).

Calibrated material parameters are shown in Table 1. The calibrated constitutive model is verified by comparing the measured behaviour to the one predicted for a one-element model built in ABAQUS. Numerical results agree with experimental data (Figure 1(b)).

3. Finite-element model

3.1. Geometry: finite-element mesh

The geometry of a typical inverted base pavement model created in ABAQUS is shown in Figure 2. Several geometric designs are generated by varying the thickness of different layers. Traffic load is modelled as a circular

Table 1. Material parameters used to represent the four layers in the finite-element model.

GAB			
Stiffness parameters	c_1^z (MPa)	130	
	c_1^y (MPa)	90	
	c_1^x (MPa)	90	
	c_2	0.45	
Poisson's ratio	ν_{xy}	0.15	
	ν_{zy}	0.35	
	ν_{zx}	0.35	
Strength parameters	c (kPa)	10	
	ϕ	57°	
AC			
CTB			
SG			
Young's modulus E	2 (GPa)	10 (GPa)	50 (MPa)
Poisson's ratio	0.35	0.2	0.2

uniform load of 650 kPa with a diameter of 300 mm which corresponds to the weight of an equivalent single axle load. The model boundaries are placed away from the load

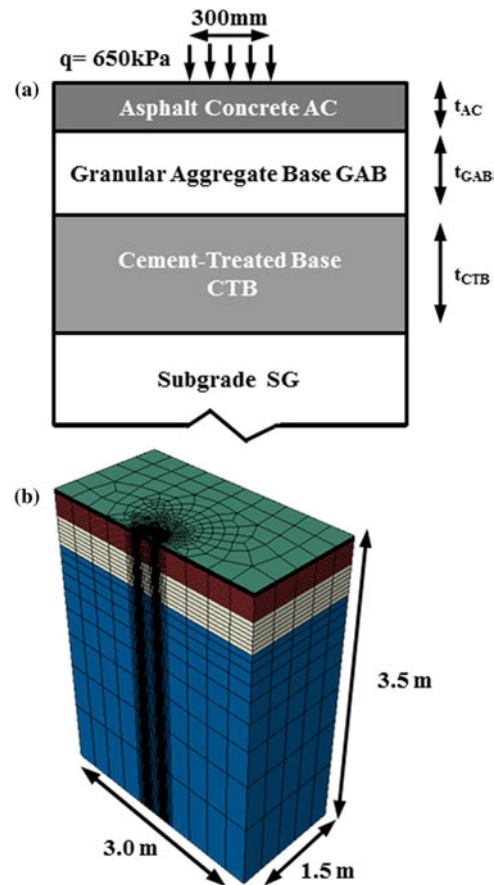


Figure 2. Numerical model. (a) Illustration of a typical inverted base pavement analysed in this study. (b) Finite-element mesh used for numerical simulations.

to minimise their influence on the analysis (verified in Cortes *et al.* 2012).

3.2. Material behaviour

Given the importance of the granular base on the response of inverted base pavements with thin-asphalt layers, the GAB layer is modelled in detail using the nonlinear stress-dependent anisotropic model described above. On the other hand, linear elasticity is selected to model the asphalt concrete, CTB and subgrade layers, in order to facilitate the interpretation of results in terms of the behaviour of the granular base. Table 1 summarises the material parameters used for all pavement layers.

3.3. Compaction-induced residual stresses

The GAB is subjected to large vertical transient stresses during compaction, and horizontal stress remains locked-in after the removal of the compaction load (Uzan 1985). Compaction-induced residual stresses are taken into consideration by assuming that the granular base moves towards a passive- K condition (Duncan and Seed 1986, Filz and Duncan 1996). Then, in the absence of traffic load, the geostatic horizontal stress σ_h^0 in the GAB is a function of the vertical geostatic stress σ_v^0 :

$$\sigma_h^0 = K_c \cdot \sigma_v^0, \quad (11)$$

where the coefficient $K_c = 6$ assumes a friction angle of 45° .

4. Results

4.1. Stress distribution

Figure 3 shows vertical and horizontal stress distributions along the load centreline for pavements of different layer thicknesses. The stiff and thick AC and CTB layers deform in bending and develop tensile horizontal stress at the bottom of the layer. The frictional GAB cannot mobilise tension; thus, the horizontal stress in the GAB is compressive everywhere. The vertical stress that reaches the subgrade is small compared to the applied stress in all cases. The effect of layer thicknesses is explored next.

4.2. Effect of AC thickness

Thicker AC layers experience lower tensile stress under the load centreline (Figure 3). As the thickness is reduced, the asphalt concrete layer transitions from a beam response to a membrane-like deformation. Thin-asphalt layers do not reduce the vertical contact stress, which is felt by the GAB with almost the same intensity. Figure 4 shows the horizontal stress along the top and bottom of the asphalt

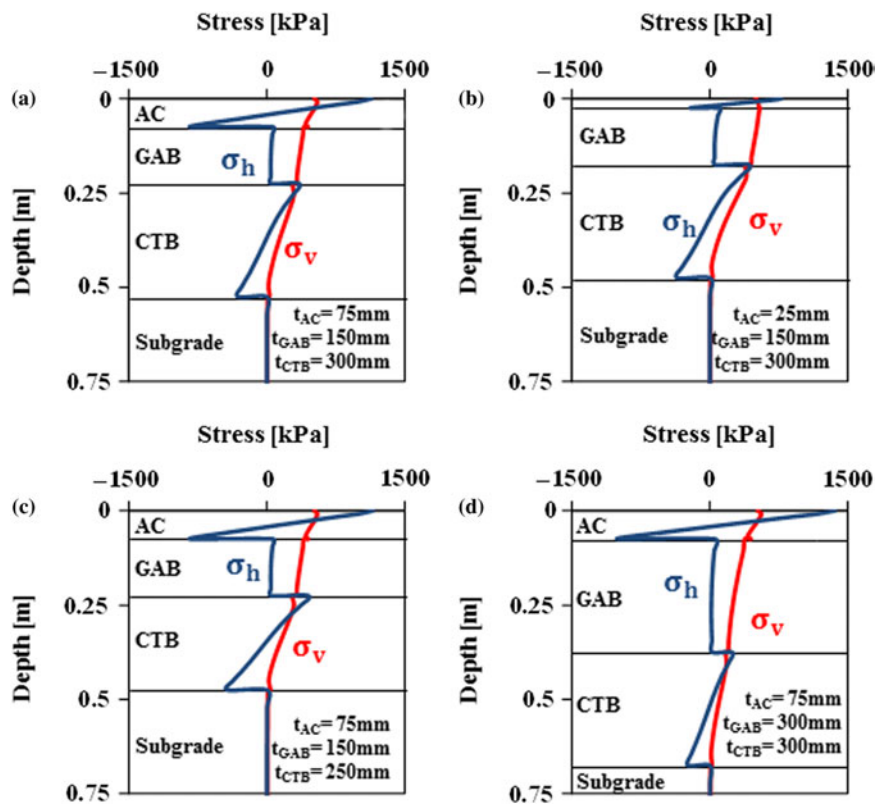


Figure 3. Vertical stress σ_v and horizontal stress σ_h distribution versus depth beneath the load centreline for different layer thicknesses.

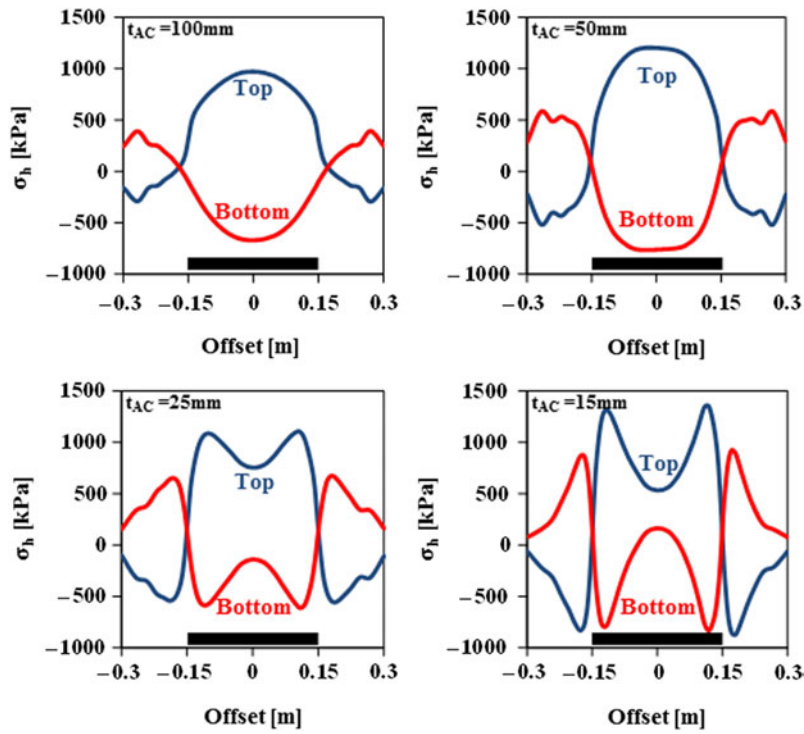


Figure 4. Horizontal stress σ_h along the top and bottom of the asphalt concrete layer for different asphalt concrete thickness. In all cases, $t_{GAB} = 150\text{ mm}$ and $t_{CTB} = 250\text{ mm}$ and the wheel load is 650 kPa . The black horizontal lines show the width of the load imprint.

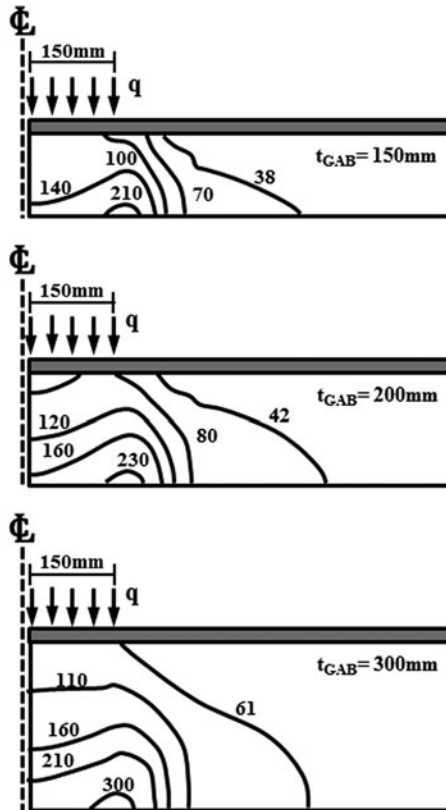


Figure 5. Stiffness contours (MPa) within the granular base under the applied wheel load $q = 650\text{ kPa}$ for different thicknesses of the granular base. In all cases, $t_{AC} = 50\text{ mm}$ and $t_{CTB} = 300\text{ mm}$.

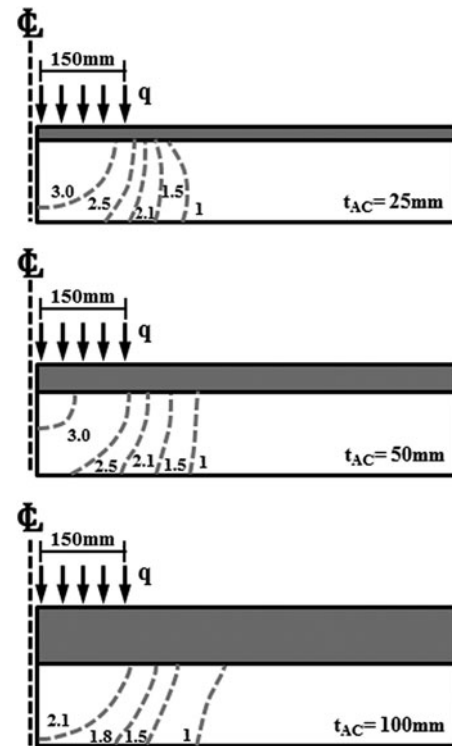


Figure 6. GAB stiffness anisotropy E_{vert}/E_{hor} contours within the granular base under the applied wheel load $q = 650\text{ kPa}$ for different thicknesses of the asphalt concrete t_{AC} . In all cases, $t_{GAB} = 150\text{ mm}$ and $t_{CTB} = 300\text{ mm}$.

concrete layer under the wheel load and for different values of asphalt concrete thickness. The maximum tensile stress is roughly the same in both cases, even though the AC layer thickness is reduced by a factor of 4. The horizontal stress profile for the 100-mm AC pavement is typical of a layer that deforms in bending as a double-fixed beam: the maximum tensile stress occurs at the bottom of the layer directly beneath the load centreline, and some tensile stress also develops at the top of the layer near the load edges. On the other hand, horizontal stresses for the 25-mm AC layer follow a different pattern: the maximum tensile stress occurs very close to the edge of the load.

4.3. Effect of GAB thickness

Thicker GAB layers increase the bending of the AC layer but decrease bending stresses in the CTB (Figure 3).

The stiffness of the GAB evolves with the state of stress as discussed above and is computed through the constitutive model described in Equations (1)–(10). Stiffness contours for different layer thicknesses are shown in Figure 5. Vertical stiffness is actually higher under the wheel load than away from the load. The proximity of the graded aggregate base to the load, along with the stiff reaction provided by the CTB, creates an effective confinement that promotes the increase in stiffness.

4.4. Effect of CTB thickness

Thinner CTB layers cause an increase in both compressive stress at the top and tensile stress at the bottom of the CTB. The responses of the AC and GAB layers are largely unaffected by the thickness of the CTB as long as this layer remains intact (Figure 3).

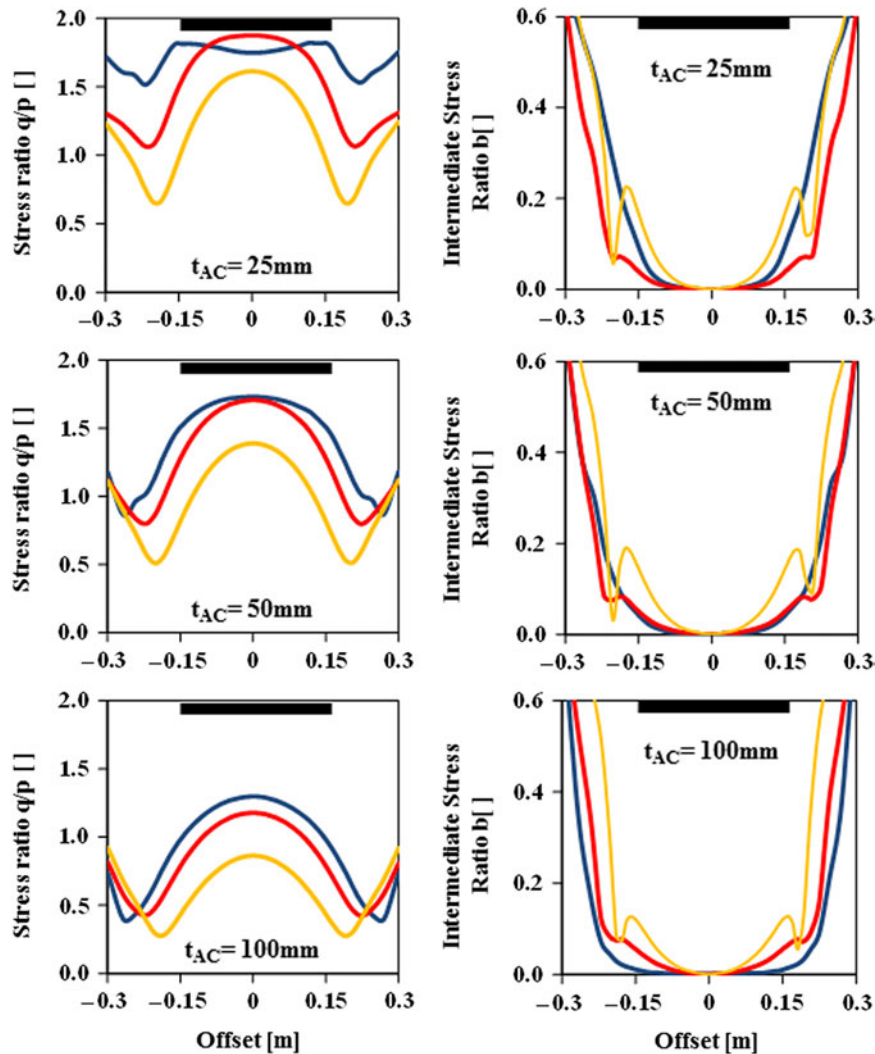


Figure 7. Stress evolution in the granular base along the wheel path. Stress ratio q/p (left column), and intermediate stress ratio $b = (\sigma_2 - \sigma_3)/(\sigma_1 - \sigma_3)$ (right column) along the centreline for different asphalt thicknesses. In all cases, $t_{GAB} = 150$ mm and $t_{CTB} = 300$ mm. The blue, red and yellow lines correspond to the top, half-depth and bottom of the GAB, respectively.

4.5. GAB stiffness anisotropy

The extent of stiffness anisotropy that develops in the GAB is showcased in Figure 6. Contours of stiffness anisotropy E_v/E_h are plotted for different asphalt concrete thicknesses. The stress sensitivity of the GAB has a large effect on the evolution of anisotropy. For a thin AC layer, the granular base is exposed to greater vertical stress and develops a higher vertical stiffness. On the other hand, a deep asphalt layer distributes the vertical contact stress over a larger area, leading to lower traffic-induced vertical and horizontal stresses. In this case, the combination of low traffic-induced stresses (mostly vertical component) and high compaction-induced residual horizontal stress results in lower stiffness anisotropy.

4.6. Observations

These results have important implications for the characterisation and modelling of pavement structures. In particular, deformations and critical responses such as tension in the AC and CTB layers and compressive stress in the subgrade can be underestimated when isotropic stiffness based on the vertically measured stiffness is assumed (Gazetas 1982). Consequently, a pseudo-isotropic model, such as the one used in mechanistic-empirical pavement design guidelines (MEPDG), needs to be properly adjusted when data used for calibration are

measured in either the horizontal or vertical direction. In addition, these results emphasise the need for a proper model and robust calibration to represent the stiffness of the GAB when thin AC layers are used.

5. Complementary analyses

5.1. Stress along the wheel path

A moving wheel load produces a complex state of stress in the pavement along the wheel path, including the rotation of the principal stresses and pronounced changes in the stress ratio. The stress ratio q/p as well as the intermediate stress ratio $b = (\sigma_2 - \sigma_3)/(\sigma_1 - \sigma_3)$ are plotted along the wheel path in Figure 7 for different asphalt concrete thicknesses. With the exception of the 25-mm AC pavement, the highest stress ratio occurs at the top of the GAB when the load is directly above the element. The principal stress direction changes dramatically along the wheel path, from triaxial extension ($\sigma_1 = \sigma_2 = \sigma_{hor}$) in the far field to almost pure triaxial compression under the load centreline ($\sigma_3 = \sigma_2 = \sigma_{hor}$). Clearly, experimental test data should include principal stress rotation.

5.2. Shear contact stress

Shear loading along the tyre–pavement interface develops under rolling conditions, during acceleration and along

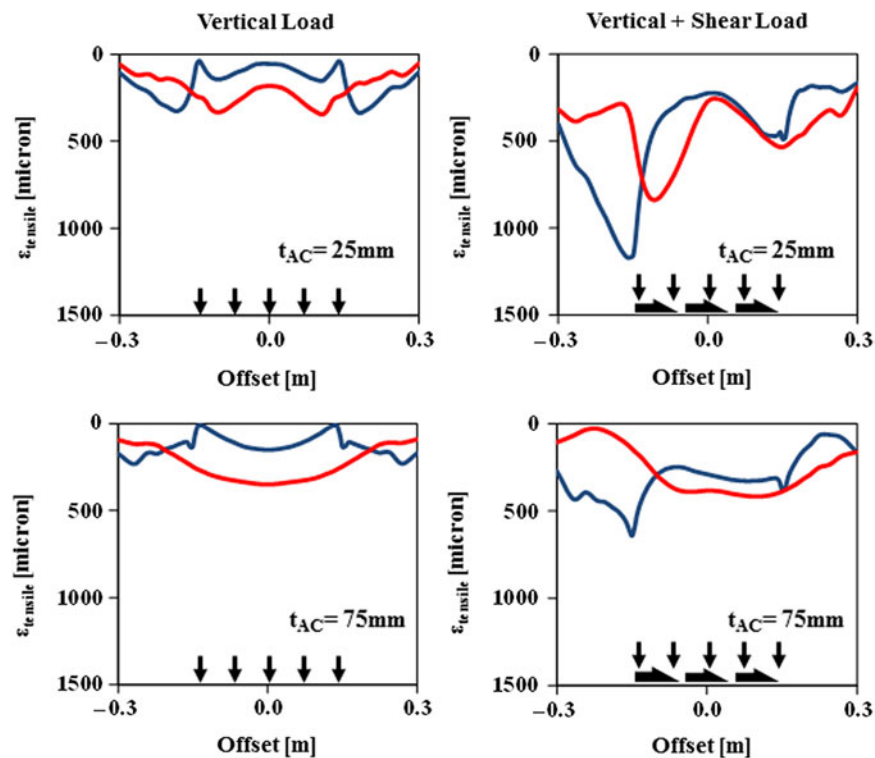


Figure 8. Tensile strain $\epsilon_{tensile}$ along the top (blue line, dark grey in print) and bottom (red line, light grey in print) of the asphalt concrete layer for purely vertical loading (left), and for combined vertical and shear contact loading (right). In all cases, $t_{GAB} = 150$ mm, $t_{CTB} = 300$ mm, the vertical contact load is 650 kPa and the contact radius $R = 150$ mm. The shear contact load assumes a friction coefficient $\mu = 1.0$.

curves (Wang 2011). While complex models are required to calculate the actual shear force on the tyre–pavement interface, the maximum mobilised shear stress can be estimated using a Coulomb friction law:

$$\tau = \mu \cdot \sigma_v, \quad (12)$$

where μ is the tyre–pavement friction coefficient.

The effect of shear stress on the response of inverted base pavements is explored by adding a shear stress component τ to the contact stress σ_v . An upper bound of $\mu = 1$ is assumed, which corresponds to a typical value for dry asphalt–tyre contact (Gustafsson 1997, Ray 1997, Muller *et al.* 2003). Figure 8 shows the tensile strain along the AC layer for the cases of only vertical load and combined vertical and shear load for two pavements with

different AC thicknesses. Contact shear increases tension at the top of the asphalt layer, at the rear end of the load imprint. In the presence of shear contact load, the benefits of a membrane response in thin AC layers may be overwhelmed by the increased tensile strain caused by the applied shear. This observation has practical implications for the design of thin AC layers in high shear zones.

5.3. AC layer thickness optimisation

Figure 9 shows critical pavement response indicators as a function of the AC and GAB thicknesses. The response of the asphalt concrete layer is sensitive to the thickness of the GAB. Both tensile and compressive strains in the AC are maximised when the thickness of the AC is

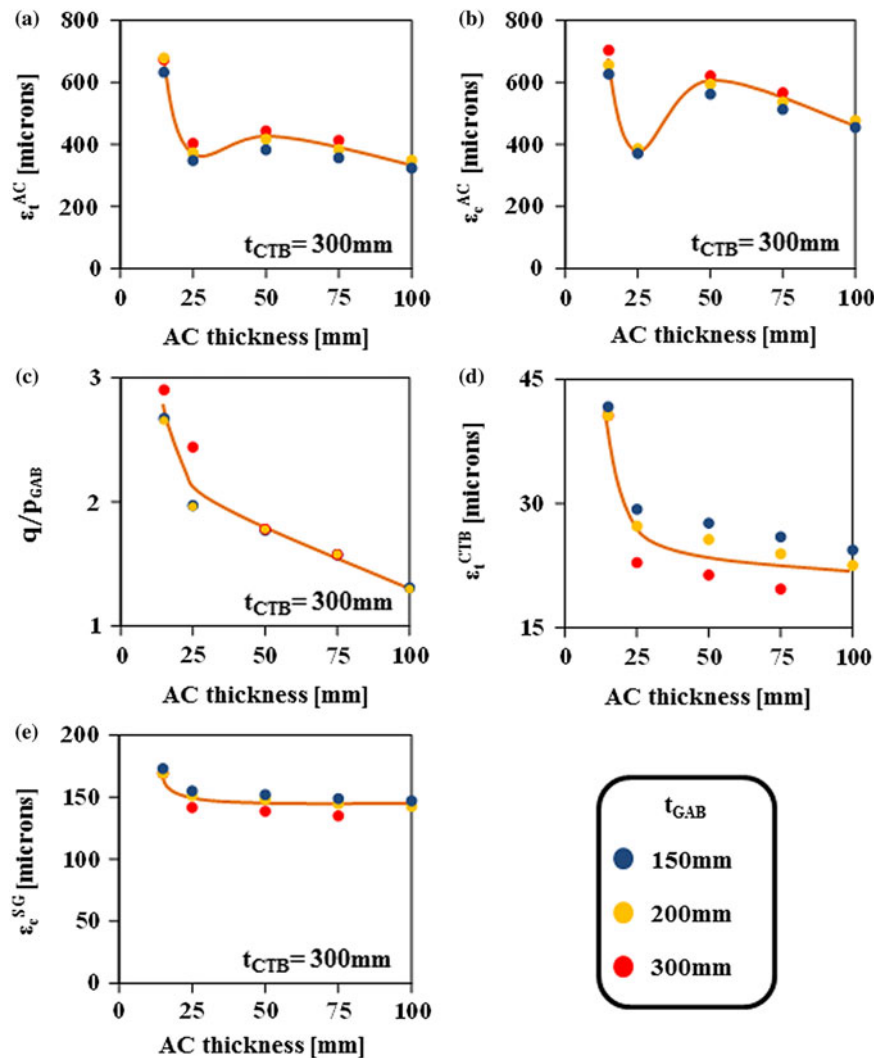


Figure 9. Maximum values of (a) AC tensile strain ϵ_t^{AC} , (b) AC compressive strain ϵ_c^{AC} , (c) stress ratio q/p in the GAB, (d) CTB tensile strain ϵ_t^{CTB} and (e) subgrade compressive strain ϵ_c^{SG} versus asphalt layer thickness for different GAB thicknesses. In all cases $t_{CTB} = 300$ mm.

50 mm (Figure 9(a),(b)); this suggests a transition thickness from a beam to a membrane deformation pattern. Nevertheless, results for tensile strain cannot be directly related to fatigue cracking. Fatigue cracking damage functions used in the MEPDG depend on layer thickness as well as tensile strain: for the same tensile strain, a 25- mm AC layer can withstand almost 10 times the amount of load repetitions compared to a 100- mm layer (NCHRP 2004). Therefore, the potential economic savings of thin AC layers for inverted base pavements include lower construction and maintenance costs as well as higher design life.

According to the MEDPG, rutting in the GAB is a function of the vertical strain. However, this correlation does not take into consideration fundamental aspects of the behaviour of geomaterials under repetitive loading such as the effect of the stress ratio q/p (Pasten *et al.* 2014). Thick AC layers spread the traffic load and help reduce the stress ratio q/p in the GAB (Figure 9(c)). The maximum tensile strain in the CTB decreases with an increase in either the GAB or the AC thickness (Figures 3, 4 and 9(d)). For example, a combination of a 25- mm asphalt concrete on top of a 300- mm GAB is equivalent to a 100- mm asphalt concrete layer over a 150- mm thick GAB. Also, the subgrade compressive strain decreases with AC thickness

(Figure 9(e)) but is mostly affected by the thickness of the GAB and CTB (not shown).

5.4. Effect of asphalt stiffness temperature

Asphalt concrete layers are particularly susceptible to temperature variations (Abbas *et al.* 2004, Kim 2009) and change from stiff-and-brittle at low temperatures to soft-and-ductile in hot weather. The temperature effect is studied by varying the stiffness of the asphalt layer. Figure 10 shows the variation of the critical pavement response parameters with asphalt thickness for different values of the asphalt layer stiffness. Lower stiffness results in lower tensile stress as well as a change in the optimal AC thickness: softer asphalt layers deform as membranes even for thicknesses as high as 50 mm, as the transition from beam- to membrane-type response is a problem of relative stiffness. On the other hand, the stress ratio in the GAB and the tensile strain in the CTB are only marginally affected by the change in AC stiffness.

5.5. Relative layer stiffness

The mechanical interactions in a three-layer pavement system can be expressed in terms of the relative stiffness π

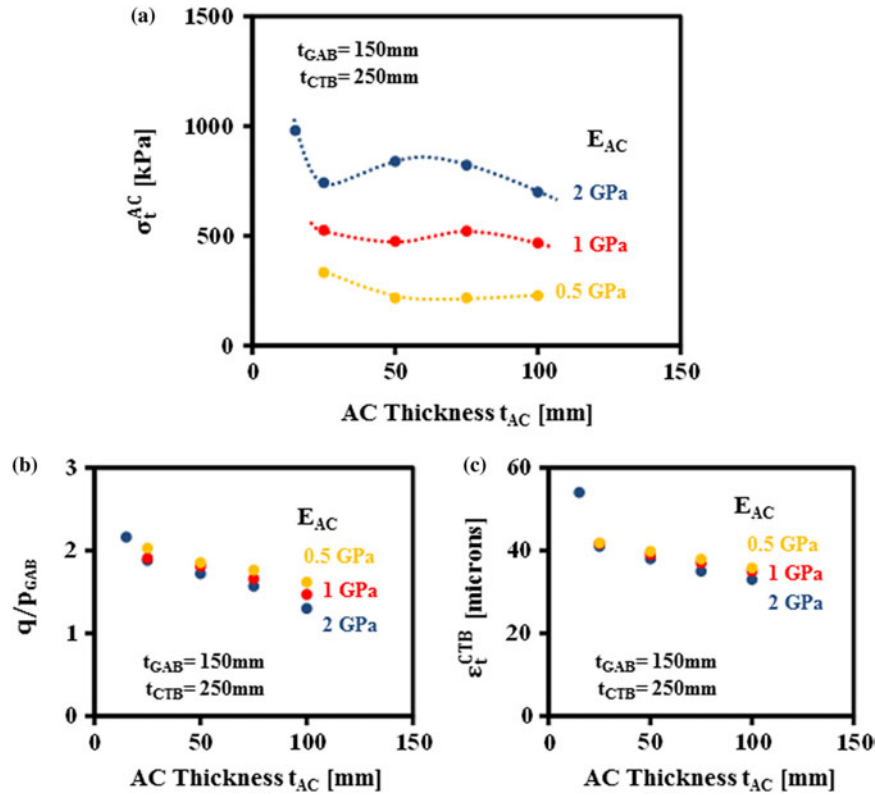


Figure 10. Effect of asphalt concrete stiffness E_{AC} . (a) Asphalt concrete tensile stress σ_t^{AC} , (b) stress ratio in the GAB q/p_{GAB} and (c) tensile strain in CTB ϵ_t^{CTB} versus asphalt concrete layer thickness t_{AC} for different values of Young's modulus in the asphalt layer E_{AC} .

between layers (Papadopoulos and Santamarina 2015). In the case of flexible pavements, these dimensionless ratios π can be defined as (Hogg 1938, Vesic 1961)

$$\pi_{AC-GAB} = \sqrt[4]{\frac{k_{AC}}{k_{GAB}}} \cdot \frac{1}{R} \quad \text{and} \quad \pi_{GAB-CTB} = \sqrt[4]{\frac{k_{GAB}}{k_{CTB}}} \cdot R. \quad (13)$$

The stiffness of each layer k_i is defined as follows (Gazetas 1983):

$$k_{AC,CTB} = \frac{E \cdot t^3}{12(1 - \nu^2)} \quad \text{and} \quad (14)$$

$$k_{GAB,SG} = \frac{3.7 \cdot E}{\pi R(1 - \nu^2)} \cdot \left(1 + 1.28 \left(\frac{R}{t} \right) \right),$$

where E is Young's modulus, ν is Poisson's ratio, t is the layer thickness and R is the radius of the load imprint.

Results from simulations analysed in this paper along with conventional pavement section simulations by Papadopoulos (2014) are plotted in terms of these dimensionless ratios in Figure 11(a). Pavement structures with a similar behaviour form clusters in this dimensionless space. Figure 11(b),(c) shows the tensile strain in the asphalt and compressive strain in the subgrade plotted against the stiffness ratios defined above. This plot shows that conventional asphalt pavements suffer considerably from subgrade deformation, while, compared to them, inverted base pavements are more prone to asphalt cracking.

6. Conclusions

A numerical three-dimensional finite-element model is used to study inverted base pavements with thin-asphalt layers using a stress-dependent constitutive model to

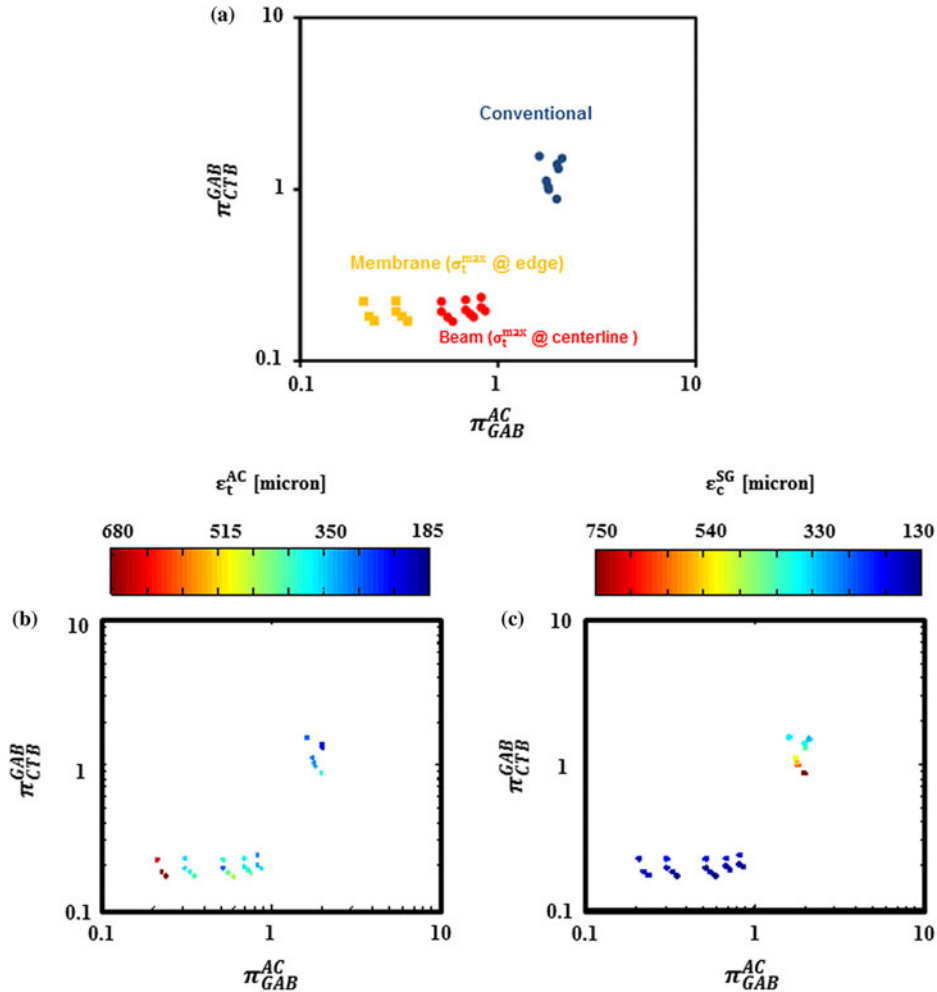


Figure 11. Relative layer stiffness in inverted base pavements. (a) Stiffness ratios between layers plotted for all pavements simulated in this study. (b) Tensile strain in the asphalt concrete layer ϵ_t^{AC} . (c) Compressive strain in the subgrade ϵ_c^{SG} versus the dimensionless stiffness ratios π .

adequately describe the behaviour of the GAB. The main conclusions from this study are as follows:

- Stress redistribution in inverted base pavements is markedly different from conventional pavements due to the stiffness contrast between subsequent layers. Stiff and thick AC and CTB layers deform as beams and develop extensive tension. The GAB acts as a cushioning layer to support the asphalt concrete layer and relieve the tension from the CTB and is under compression everywhere. The subgrade is largely unaffected by the load. There is no universally acceptable thickness of any layer. Therefore, each inverted base pavement needs to be engineered to match the traffic intensity and environmental conditions at hand.
- Thin-asphalt concrete layers deform as membranes rather than beam elements. As the thickness decreases, the tensile strain decreases at the bottom of the layer, but it increases at the edges of the load. In order to benefit from this behaviour, the AC thickness must not exceed 25–50 mm, depending on the weather conditions. Thin AC inverted base pavements develop relatively low tensile strains which lead to longer fatigue life and, combined with the low cost of a thin layer, economic savings.
- The stiffness of the granular base is stress dependent. Thus, there are marked changes in the stiffness of the granular layer during the application of traffic load, particularly when thin AC layers are used. The inherent and stress-induced anisotropy of the base requires careful laboratory protocols to measure the behaviour and adequate constitutive models to represent it.
- Shear contact stresses due to acceleration and braking increase the tension in the AC layer, particularly when a thin AC layer is used.
- The response of pavement structures can be classified in terms of the relative stiffness between successive layers. Inverted base pavements are not prone to develop permanent deformation in the subgrade. However, the asphalt layer can be susceptible to fatigue cracking.

Funding

The Georgia Department of Transportation and the Georgia Construction Aggregate Association under its executive director John Cardosa funded this research. Additional support was provided by the Goizueta Foundation.

References

Abbas, A.R., Papagiannakis, A.T., and Masad, E.A., 2004. Linear and nonlinear viscoelastic analysis of the microstructure of

- asphalt concretes. *Journal of Materials in Civil Engineering*, 16 (2), 133–139.
- Al-Qadi, I.L., Wang, H., and Tutumluer, E., 2010. Dynamic analysis of thin asphalt pavements by using cross-anisotropic stress-dependent properties for granular layer. *Transportation Research Record*, 2154, 156–163.
- Barksdale, R.D., Brown, S.F., and Chan, F., 1989. *Potential benefits of geosynthetics in flexible pavement systems*. Washington, DC: Transportation Research Board, NCHRP Report No. 315.
- Brown, S.F., 1996. Soil mechanics in pavement engineering. *Geotechnique*, 46 (3), 381–426.
- Brown, S.F. and Pappin, J.W., 1981. Analysis of pavements with granular bases. *Transportation Research Record*, 810, 17–23.
- Burmister, D.M., 1945. The general theory of stresses and displacements in layered systems. I. *Journal of applied physics*, 16 (2), 89–94.
- Burmister, D.M., *et al.*, 1943. The theory of stress and displacements in layered systems and applications to the design of airport runways. In: *Proceedings of the twenty-third annual meeting of the highway research board held at Edgewater Beach Hotel, Chicago, IL, 27–30 November*.
- Cortes, D.D., 2010. *Inverted base pavement structures*, Ph.D. Georgia Institute of Technology, Atlanta, GA.
- Cortes, D.D. and Santamarina, J.C., 2013. The LaGrange case history: inverted pavement system characterisation and preliminary numerical analyses. *International Journal of Pavement Engineering*, 14 (5), 463–471.
- Cortes, D.D., Shin, H., and Santamarina, J.C., 2012. Numerical simulation of inverted pavement systems. *Journal of Transportation Engineering*, 138 (12), 1507–1519.
- Duncan, J.M., Monismith, C.L., and Wilson, E.L., 1968. Finite element analyses of pavements. *Highway Research Record*, 228, 18–33.
- Duncan, J.M. and Seed, R.B., 1986. Compaction-induced earth pressures under K0-conditions. *Journal of Geotechnical Engineering*, 112 (1), 1–22.
- Fahey, M. and Carter, J.P., 1993. A finite element study of the pressuremeter test in sand using a nonlinear elastic plastic model. *Canadian Geotechnical Journal*, 30 (2), 348–362.
- Filz, G.M. and Duncan, J.M., 1996. Earth pressures due to compaction: comparison of theory with laboratory and field behavior. *Transportation Research Record*, 1526, 28–37.
- Garg, N. and Thompson, M.R., 1997. Triaxial characterization of Minnesota Road Research project granular materials. *Transportation Research Record: Journal of the Transportation Research Board*, 1577 (1), 27–36.
- Gazetas, G., 1982. Stresses and displacements in cross-anisotropic soils. *Journal of the Geotechnical Engineering Division*, 108 (4), 532–553.
- Gazetas, G., 1983. Analysis of machine foundation vibrations: state of the art. *International Journal of Soil Dynamics and Earthquake Engineering*, 2 (1), 2–42.
- Gustafsson, F., 1997. Slip-based tire–road friction estimation. *Automatica*, 33 (6), 1087–1099.
- Hardin, B.O. and Drnevich, V.P., 1972b. Shear modulus and damping in soils: design equations and curves. *Journal of Soil Mechanics and Foundations Div*, 98 (SM7), 667–692.
- Hicks, R.G. and Monismith, C.L., 1971. Factors influencing the resilient response of granular materials. *Highway Research Record*, 345, 15–31.
- Hogg, A., 1938. Equilibrium of a thin plate, symmetrically loaded, resting on an elastic foundation of infinite depth. *The London, Edinburgh, and Dublin Philosophical Magazine and*

- Journal of Science*, 25 (168), 576–582.
- Kim, M., Tutumluer, E., and Kwon, J., 2009. Nonlinear pavement foundation modeling for three-dimensional finite-element analysis of flexible pavements. *International Journal of Geomechanics*, 9 (5), 195–208.
- Kim, Y.R., 2009. *Modeling of asphalt concrete*. New York, NY: McGraw-Hill.
- Kopperman, S.E., Stokoe, K.H., and Knox, D.P., 1982. *Effect of state of stress on velocity of low-amplitude compression waves propagating along principal stress directions in dry sand*. Washington, DC: Air Force office of Scientific Research, Bolling AFB, Technical report.
- Liu, Q. and Shalaby, A., 2013. Simulation of pavement response to tire pressure and shape of contact area. *Canadian Journal of Civil Engineering*, 40 (3), 236–242, doi:10.1139/cjce-2011-0567.
- Mayne, P.W., 2001. Stress–strain–strength–flow parameters from enhanced *in-situ* tests. In: *Proceedings of international conference on in situ measurement of soil properties and case histories*, 21–24 May 2001, Bali, Indonesia, 27–47.
- Muller, S., Uchanski, M., and Hedrick, K., 2003. Estimation of the maximum tire–road friction coefficient. *Journal of Dynamic Systems, Measurement, and Control*, 125 (4), 607–617.
- NCHRP, 2004. *Guide for mechanistic-empirical design of new and rehabilitated pavement structures*. N.R. Council ed. Washington, DC: NCHRP.
- Oda, M., Nemat-Nasser, S., and Konishi, J., 1985. Stress-induced anisotropy in granular masses. *Soils and Foundations*, 25 (3), 85–97.
- Papadopoulos, E., 2014. *Performance of unbound aggregate bases and implications for inverted base pavements*, Ph.D. Georgia. Institute of Technology, Atlanta.
- Papadopoulos, E., Cortes, D.D., and Santamarina, J.C., 2015. *In situ* assessment of the stress-dependent stiffness of unbound aggregate bases: application in inverted base pavements. *International Journal of Pavement Engineering*, under review.
- Papadopoulos, E. and Santamarina, J.C., 2015. Inverted base pavements: construction and performance. *Journal of Transportation Engineering*, under review.
- Park, S.W. and Lytton, R.L., 2004. Effect of stress-dependent modulus and Poisson's ratio on structural responses in thin asphalt pavements. *Journal of Transportation Engineering*, 130 (3), 387–394.
- Pasten, C., Shin, H., and Santamarina, J., 2014. Long-term foundation response to repetitive loading. *Journal of Geotechnical and Geoenvironmental Engineering*, 140 (4), 04013036.
- Prevost, J.H. and Keane, C.M., 1990. Shear stress–strain curve generation from simple material parameters. *Journal of geotechnical Engineering*, 116 (8), 1255–1263.
- Raad, L. and Figueroa, J.L., 1980. Load response of transportation support systems. *Journal of Transportation Engineering*, 106 (1), 111–128.
- Ray, L.R., 1997. Nonlinear tire force estimation and road friction identification: simulation and experiments. *Automatica*, 33 (10), 1819–1833.
- Santamarina, J.C., Klein, K., and Fam, M.A., 2001. *Soils and waves: particulate materials behavior, characterization and process monitoring*. New York, NY: Wiley & Sons Ltd.
- Terrell, R.G., et al., 2003. Field evaluation of the stiffness of unbound aggregate base layers in inverted flexible pavements. *Transportation Research Record*, 1837 (2003), 50–60.
- Tutumluer, E., 2013. Practices for unbound aggregate pavement layers. *Synthesis*, NCHRP, ed.
- Tutumluer, E. and Barksdale, R.D., 1995. Behaviour of pavements with granular bases-prediction and performance. In: *Proceedings of the fourth international symposium on unbound aggregates in roads*, Nottingham, UK, 173–183.
- Uzan, J., 1985. Characterization of granular material. *Transportation Research Record*, 1022 (1), 52–59.
- van Niekerk, A.A., Molenaar, A.A.A., and Houben, L.J.M., 2002. Effect of material quality and compaction on the mechanical behaviour of base course materials and pavement performance. In: *6th international conference on bearing capacity of roads, railways and airfields*, 24–26 June 2002, Lisbon, 1071–1079.
- Vesic, A., 1961. Bending of beams resting on isotropic elastic solid. *Journal of Soil Mechanics and Foundation Engineering, ASCE*, 87 (2), 35–53.
- Wang, H., 2011. *Analysis of tire–pavement interaction and pavement responses using a decoupled modeling approach*. Urbana, IL: University of Illinois.
- Yoo, P.J., et al., 2006. Flexible pavement responses to different loading amplitudes considering layer interface condition and lateral shear forces. *The International Journal of Pavement Engineering*, 7 (1), 73–86.